ACS APPLIED MATERIALS & INTERFACES

www.acsami.org
Research Article

Membrane-Targeted Quantum Dot-Based BACE1 Activity Sensors for *In Vitro* and *In Cellulo* Assays

Carlota Tosat-Bitrián, Jesús Alejandro Bueso de Barrio, Michael H. Stewart, Kimihiro Susumu, Igor L. Medintz, Sebastián A. Díaz,* and Valle Palomo*

Cite This: *ACS Appl. Mater. Interfaces* 2024, 16, 63186−63194
Read Online

ABSTRACT: The need for the development of specific and robust methodologies to elucidate the intricate pathological mechanisms of neurodegenerative diseases and discover effective treatments for prevention and remediation is evident. Alzheimer's disease, in particular, has become more prevalent as the global population has aged. β-Secretase, the β-site amyloid precursor protein cleaving enzyme (BACE1), is the protease that produces the β-amyloid peptide, which is considered one of the driving factors of Alzheimer's disease and an important target for treatment development. However, an understanding of its activity, modulation, and regulation is far from complete. This is in large part due to the complex nature of following its activity. Beyond the common requirements for all biosensors (ease of preparation and use), BACE1 probes also demand both stability at acidic pH and membrane localization. To overcome these hurdles, we exploit the modular self-assembly provided by fluorescent quantum dot (QD) sensors. As compared to other fluorophores, QDs provide enhanced fluorescence brightness and photostability, and their large surface area enables functionalization with peptide substrates together with targeting elements that localize the sensor to the areas of maximal BACE1 activity, all achieved through His-tag self-assembly. *In vitro*, the sensor demonstrated stability under acidic conditions, and using high-throughput plate reader assays, we determined BACE1 activity in-line with literature values and enabled the obtainment of the inhibitor constant of verubecestat, a small molecule inhibitor. The sensor was also transitioned to cellular experiments, where it demonstrated sensitivity to BACE1 activity and its modulation upon inhibitor treatment in a neuroblastoma cell line.

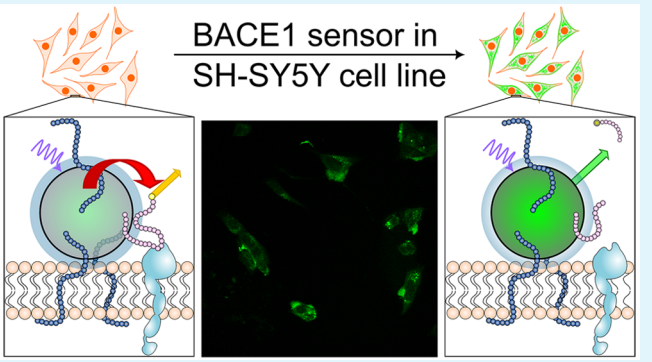

KEYWORDS: *BACE1, protease, quantum dots, FRET sensor, Alzheimer's disease, drug discovery*

INTRODUCTION

β-Site amyloid precursor protein cleaving enzyme (BACE1), or β-secretase, is a membrane aspartic acid protease highly expressed in the brain, specifically in neuronal tissue. It has a single transmembrane domain, and while it is located at the extracellular membrane of the cell, its optimal activity is found in lower pH late endosomes, ranging from pH 4 to 5.[1] This enzyme has been intensely studied due to its key role in Alzheimer's disease pathogenesis. Specifically, BACE1 is responsible for the hydrolytic generation of the β-amyloid peptide, as determined by excising the amyloid precursor protein (APP) found on the senile plaques observed in patient's brains post-mortem. Aside from β-amyloid production, BACE1 has other functionalities that play positive roles in brain health, such as in the remyelination of axons,[2] synaptic function,[3] neurogenesis,[4] and insulin signaling.[5] In addition, some studies have found that BACE1 might be involved in other neurodegenerative diseases.[6,7] The pathological contribution of BACE1 has motivated the generation of BACE1 inhibitors that demonstrated significant reduction of β-amyloid formation in animal models and also human patients.[8,9] However, the complete understanding of this enzyme's role in pathology remains unclear, and while some inhibitors have shown promising results in clinical studies others have been halted even after reaching advanced phases of clinical development.[10]

Developing a sensor that accurately monitors BACE1 activity in living cells entails several additional technical hurdles that need to be overcome in order to obtain a physiological readout of the protease activity. BACE1 is a membrane-bound protease, primarily excising membrane-bound substrates located at the plasma membrane, endosome, and the Golgi apparatus.[11] Therefore, the precise location of

Received: July 26, 2024
Revised: September 5, 2024
Accepted: September 6, 2024
Published: November 8, 2024

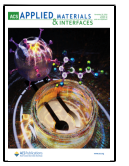

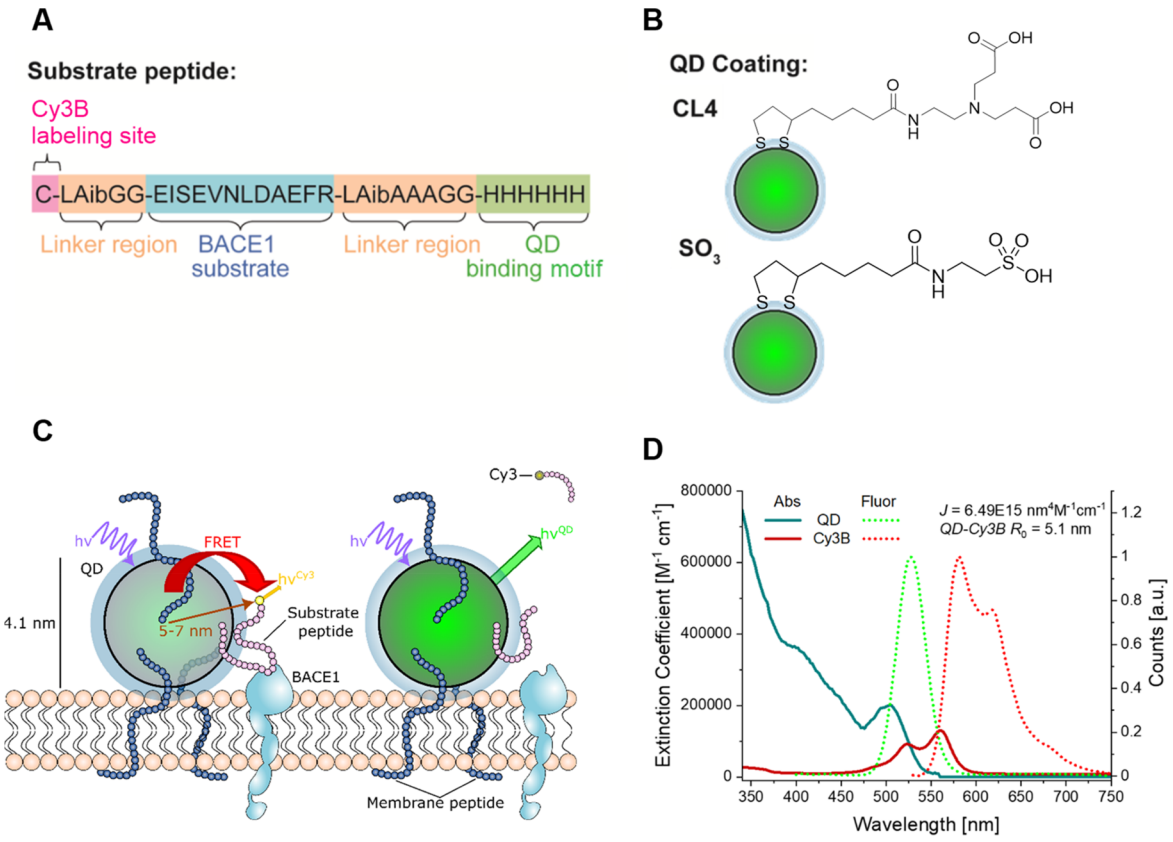

Figure 1. Schematic representation of the structure and fluorescence spectra of QD and the Cy3B-labeled substrate peptide. (A) Peptide sequence of the BACE1 substrate peptide with its functional regions differentiated by color, Cy3B labeling site (pink), linker region (orange), BACE1 substrate (blue), and QD binding motif (green). (B) Display of the two different QD coatings, CL4 and SO_3. (C) Schematic of the sensor and its function. (D) Spectral properties of the QD and Cy3B, including spectral overlap J and Förster distance R_0. The R_0 was calculated assuming $\kappa^2 = 2/3$, $n = 1.33$, and a QD quantum yield (QY) = 0.20.

the sensor within the cell is key to determining the enzyme activity at the fundamental site of action. The second requirement is sensor stability at the enzyme working conditions, which in this case entails an acidic pH of 4.5.[1] Having a reliable and sensitive BACE1 sensor that can be used in living cells would offer real-time information about different biological processes, and the cell-wide effects of its inhibition could be determined. Moreover, it would open the possibility of examining the behavior of several classes of inhibitors downstream, studying both BACE1 activity and related side effects. Understanding these effects could also highlight clues for the development of improved BACE1 inhibitors or could yield effective methodologies for early diagnosis of neurodegenerative diseases.[12]

Given the relevance of the target, several groups have developed fluorescent biosensors for monitoring BACE1 activity and its intracellular distribution.[13−16] These sensors are generally based on organic molecules or fluorescent proteins that, given their suboptimal fluorescence characteristics, limit the detection capability. Furthermore, they have generally not been optimized to location and pH. To date, due to their limitations, these studies have not provided quantitative information about the possible effects of BACE1 inhibition by small molecules.

Quantum dots (QDs) are luminescent semiconductor nanoparticles. QDs are utilized for their unique photophysical characteristics, such as broad excitation, sharp emission, high quantum yield (QY), resistance to photobleaching, and high molar extinction coefficients. These properties, along with their 3−6 nm diameter size, make them optimal imaging probes as well as donors for Förster Resonance Energy Transfer (FRET)-based assays.[17−20] FRET is the nonradiative energy transfer from the excited state of a donor fluorophore, in this case the QD, to the ground state of an acceptor molecule, which can be a dark quencher or a red-shifted emission fluorophore. Many in-depth reviews exist on the topic of QD FRET, and we direct the reader there.[18] A few key facts worth highlighting are that the energy transfer results in changes in the fluorescence lifetimes and overall fluorescence intensity of the donor and acceptor, allowing the FRET efficiency to be correlated through fluorescence spectra. The other important property of FRET is that its efficiency decays with an inverse sixth power dependence on donor−acceptor distance and typically is sensitive to distance changes in the 1−10 nm range. The classic QD sensor, in line with what we have designed for BACE1, has multiple copies of a dye-labeled substrate bound near the QD surface resulting in high FRET efficiency.[20,21] If the enzyme is present, it can cleave the substrate allowing the acceptor dye to diffuse from the QD surface, reducing FRET.[22−25] This is seen as an increase in QD fluorescence and a decrease in the sensitized fluorescence of the acceptor dye.

In addition to the aforementioned photophysical properties, QDs have another important benefit. Their large surface area can be tailored to provide stability in diverse mediums, and additional functionalities, beyond just the enzyme substrate,

https://doi.org/10.1021/acsami.4c12560
ACS Appl. Mater. Interfaces 2024, 16, 63186−63194

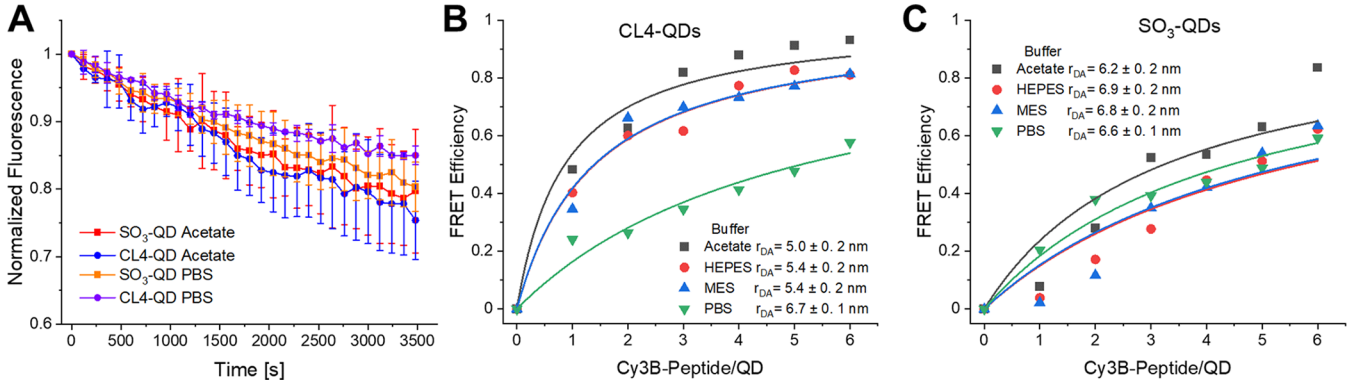

Figure 2. Stability and quenching efficacy of CL4-QD and SO_3-QD in different buffers. (A) Colloidal stability of SO_3-QD and CL4-QD in sodium acetate (50 mM, pH 4.5) or PBS (1X, pH 7.0) buffers. Fluorescence emission intensity at 545 nm was recorded every 2 min for 60 min and normalized to the first data point for each condition. Data are represented as mean ± SD. (B) FRET efficiency of the CL4-QDs as a function of the number of Cy3B-labeled peptides and the aqueous buffer. (C) FRET efficiency of the SO_3-QDs as a function of the number of Cy3B-labeled peptides and the aqueous buffer. The donor−acceptor distance r_{DA} is obtained from the FRET curves (fits-solid lines) and provided in the legend for both CL4-QDs and SO_3-QDs.

can be appended to the QD. Furthermore, this can be done in a simple self-assembly manner through the inclusion of His-tags that self-assemble to the Zn ions on the QD surface.[26] Choosing the correct surface ligands has allowed the development of low-pH stable QDs,[27] which makes them ideal systems to probe an acidic pH working enzyme with strong luminescence. Choi and colleagues have reported a BACE1 sensor using QDs as fluorophores.[28] However, this sensor lacked the two key aspects to form an optimal BACE1 sensor: (i) the absence of a membrane anchoring motif to keep the sensor at its physiological location proven to be crucial for BACE1 monitoring, and (ii) there was no evidence of the sensor performance in acidic pH, which is one of the limitations of standard QDs. We utilize the large QD surface area to self-assemble a membrane targeting peptide, JB858, that has been shown to remain in the membrane and localize QDs for more than 48 h.[29]

Here we have successfully developed a QD-based BACE1 sensor that is stable at acidic pH and is not perturbed when membrane anchor molecules are introduced. The sensor is based on a QD donor that undergoes FRET to a fluorescently labeled peptide substrate for BACE1. Presence of the enzyme results in cleavage of the peptide and a change in the ratiometric fluorescent signal. Importantly through the modular design provided in our QD-based sensor, e.g., inclusion or not of membrane targeting peptide, we can quickly oscillate from a minimalist high-throughput *in vitro* screening assay for inhibitor candidates to corroborate the candidate *in cellulo* using the fully formed sensor. We demonstrated quantification of BACE1 activity *in vitro* and determination of an inhibitor constant, K_i, of a known small molecule inhibitor (verubecestat). Subsequently, we demonstrated the sensor's turn-on capability in response to BACE1 activity in live cells, along with its fluorescence response to adding the inhibitor to the cellular medium.

RESULTS AND DISCUSSION

Design and Synthesis of the QD-BACE1 Sensor. Based on the design of previous QD FRET-based sensors for monitoring protease activity,[21,23] a peptide substrate was designed in a modular manner. The peptide contained a 12 amino acid sequence derived from the Swedish mutant APP sequence EISEVNL↓DAEFR (↓ represents the cleavage site), which has shown to be efficiently cleaved by BACE1,[30] flanked by α-helical regions (LAibGG/LAibAAAGG) needed for protease activity.[31] This substrate peptide was first labeled at the N-terminus with the organic fluorophore Cy3B, chosen over the more common Cy3 dye due to increased brightness and stability,[32] through a maleimide−thiol reaction and then assembled to QD surface through a His-tag (His_6) on the C-terminus that promotes self-assembly on the QD surface (Figure 1A).[26]

The QDs have a CdSe/CdS/ZnS core/shell/shell structure with a diameter of 4.7 ± 0.4 nm, as synthesized in house and characterized in previous works.[33,34] In order to improve QD colloidal stability at lower pH, two different QD surface coatings were tested, both based off of a bidentate dihydrolipoic acid anchor group with either a zwitterionic head (CL4) or a sulfonate head (SO_3) (Figure 1B).[27] The CL4 ligand has shown stability up to the desired pH value of 4, while the SO_3 would provide an alternative, capable of withstanding lower pH if CL4 proved to be unfeasible. The QD combined with the Cy3B had good spectral overlap (Figure 1D), and as a donor−acceptor FRET pair their Förster distance, R_0, which is the distance at which FRET efficiency is 50%, was 5.1 nm. Taking into account the multiple Cy3B acceptors that could be added to the central QD donor surface resulted in FRET efficiencies regularly above 75−80% due to the proportional increase in FRET acceptor cross-section.

The stability of both types of QDs was determined in two buffers at different pH, sodium acetate buffer (pH 4.5) and phosphate-buffered saline (PBS, pH 7.0), by monitoring fluorescence at their emission maximum wavelength, 545 nm, over time. As seen in Figure 2A, SO_3-QDs have a similar stability in both buffers while CL4-QD showed slightly less stability in sodium acetate than PBS, though only a 10% decrease.

To determine the optimal sensor, we looked at the FRET efficiency of the two QDs at different pH values, ranging from 4 to 7, and varying ratios of Cy3B-peptide to QD (1−6:1). What was observed was that the CL4-QDs followed the centrosymmetric multi-acceptor FRET efficiency dependency predicted by theory[18] (except in PBS), while the SO_3-QDs had less FRET efficiency overall along with strong deviations from the typical FRET curve. It has been shown that the choice of

https://doi.org/10.1021/acsami.4c12560
ACS Appl. Mater. Interfaces 2024, 16, 63186−63194

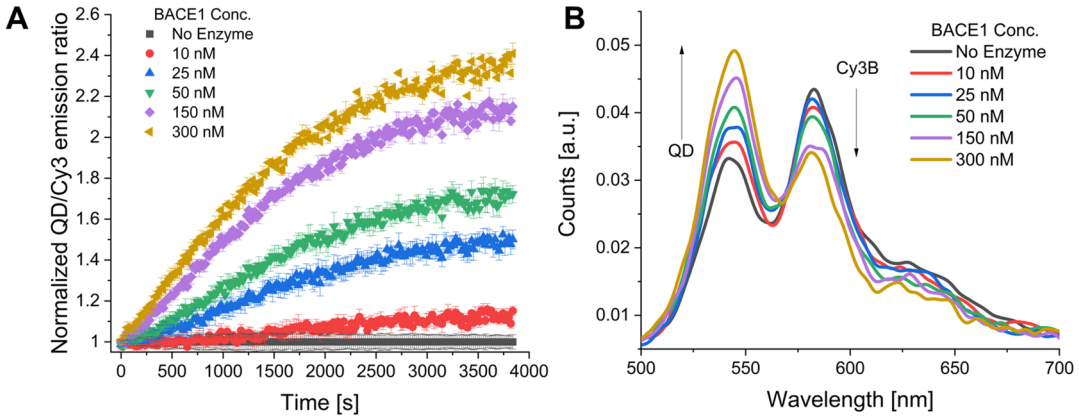

Figure 3. BACE1 kinetic assay. BACE1 activity was determined by monitoring the fluorescence emission of QD at 545 nm and Cy3B at 580 nm every 20 s for 60 min. (A) The ratio QD/Cy3B was normalized to the condition with no enzyme, observing an increase dependent on the BACE1 concentration. Data are represented as mean ± SD. (B) The emission spectra of each condition was recorded at the end point of the reaction. Each condition was run in triplicate.

QD surface ligand can modify the structure of surface-bound peptides,[35,36] so it is possible that the SO_3-QDs modified the normal structure of the substrate peptide. For the CL4-QDs the maximum quenching efficacy was reached in sodium acetate buffer at pH 4.5 (93%) obtaining similar values in 4-(2-hydroxyethyl)-1-piperazineethanesulfonic acid (HEPES) (82%) and 2-(*N*-morpholino)ethanesulfonic acid (MES) (82%), but not in PBS (57%) (Figure 2B). As the pI of the peptide is 6.05, it could be that the total net charge of the peptide at acidic pH is facilitating their assembly onto the QDs, or again, a structural modification of the peptide might be occurring at the differing pH. Due to the higher value in FRET efficiency and only slightly decreased QD stability, subsequent experiments were undertaken using the CL4-QD. In order to increase the stability of the CL4-QDs and avoid nonspecific interactions with the enzyme, a blocking peptide (HHHHHHGWDDD) composed of a short negatively charged peptide along with a His-tag was also assembled to the QD surface.[37] An optimization experiment is available in the Supporting Information, from which we determined that the optimal result was obtained with the addition of 20 blocking peptides per QD (Figure S3).

BACE1 Kinetic Assay. Once we had characterized the FRET efficacy of our sensor, a kinetic assay was performed to monitor BACE1 activity. First, different conditions were tested to optimize the BACE1 kinetic assay with two enzyme concentrations (150 nM, 300 nM): (i) assay buffer (acetate or HEPES), (ii) number of equivalents of labeled peptide per QD (2 or 4), (iii) order of reagents addition (enzyme added to sensor or sensor added to enzyme); (iv) and presence of a detergent to improve the stability of the system (Tween-20 0.1%). After these assays (quantification presented in Table S1 in the Supporting Information), the optimal conditions for the kinetic assays were determined to be the following: acetate buffer at pH 4.5, 4 equiv of labeled peptide per QD, and no detergent was added as it did not significantly improve the efficacy of the enzyme. The order of reagent addition did not modify the efficacy of BACE1 assay.

We then proceeded to confirm the utility of our sensor for the BACE1 activity. As can be seen in Figure 3, a range of BACE1 concentrations (0, 10, 25, 50, 150, 300 nM) were tested against a fixed concentration of sensor (15 nM). The fluorescence emission ratio of the QD over Cy3B increases over time in the presence of BACE1, which indicates that the peptide is being cleaved and diffusing away from the surface of the QD, diminishing FRET efficiency. The emission spectra were recorded at the end point of the reaction (60 min), confirming the ratiometric change of the QD and Cy3B emission (Figure 3B). At the 30 min mark, a limit of detection (LOD) around 10 nM was obtained for the assay *in vitro*, while at 60 min the 10 nM concentrations were above the 3σ of the baseline and the LOD was somewhere between 5 and 10 nM of BACE1.

From the data, and using enzymatic progress curves with a fixed substrate and varied enzyme concentration modality,[21] the specificity constant of BACE1 (k_{cat}/K_M) was calculated for the Cy3B-labeled BACE1 substrate peptide, and a k_{cat}/K_M = 3.2 ± 1.7 mM^{-1} s^{-1} was obtained by fitting to the Michaelis–Menten equation. This value is in agreement with previously reported k_{cat}/K_M values for different BACE1 peptide substrates that range from 1.3 to 4.5 mM^{-1} s^{-1};[30] this signifies that the steric hindrance of the QD does not limit BACE1 activity. We note that the sensor did not include the membrane anchor peptide at this time.

To confirm the sensor capability to assay BACE1 activity modifiers, we proceeded to validate the sensor by using a commercial inhibitor of BACE1, verubecestat (K_i: 2.2 nM).[38] A wide range of drug concentrations was tested, from 0.01 to 10 nM, to elaborate an inhibition curve and experimentally calculate the K_i value. We found a dose-dependent inhibition for the compound, observing almost total inhibition of the enzyme at concentrations higher than 10 nM (Figure 4). An estimated K_i value in the range of 2.0 ± 0.2 nM was obtained, being similar to previous published data.[38] These results further validate the specificity of the sensor to determine BACE1 activity and show the potential for using the sensor for high-throughput testing of BACE1 modifiers *in vitro*.

Construction of a Membrane-Bound QD FRET-Based Sensor. Another important challenge when developing a BACE1 sensor for application to live cell monitoring is to ensure that the sensor will be membrane-bound in living cells since it has been shown that APP constructs that lack the transmembrane domain are not cleaved when transfected into cells.[39] This evidence suggests that the peptide must be membrane-bound in order to undergo hydrolytic cleavage by BACE1. There are several strategies for membrane anchoring

https://doi.org/10.1021/acsami.4c12560
ACS Appl. Mater. Interfaces 2024, 16, 63186−63194

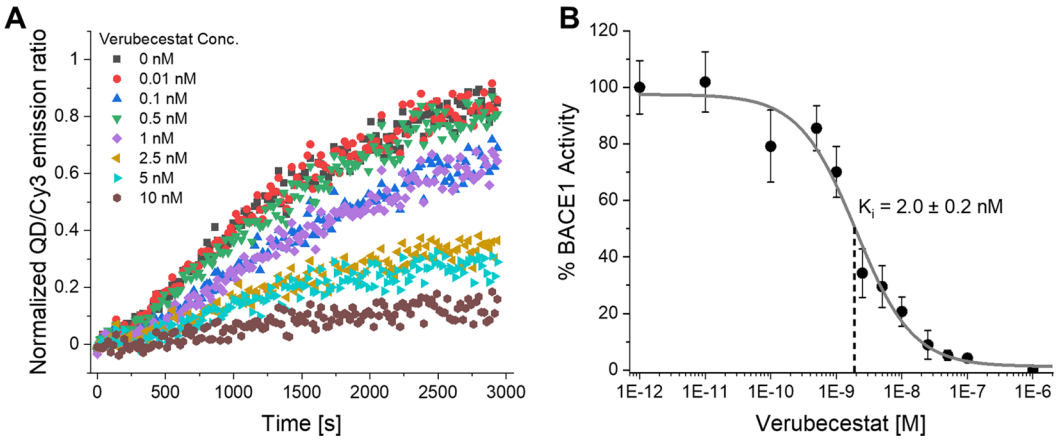

Figure 4. Different concentrations of BACE1 inhibitor verubecestat, 0, 0.01, 0.1, 0.5, 1, 2.5, 5, and 10 nM, were assayed to determine the specificity of the reaction. (A) Time trace of QD/Cy3B as a function of the verubecestat concentration. (B) An inhibition curve was plotted by representing the BACE1 activity against the concentration of verubecestat (log scale). Uncertainties arise from triplicate samples. Data are represented as mean ± SD.

of nanoparticles or macromolecules, the most advantageous being hydrophobic anchoring using determined lipophilic moieties frequently based on phospholipids. Based on previously published studies, we selected the JB858 peptide, which contains a palmitoyl moiety, to anchor the sensor to the membrane, as it was proved that QDs conjugated with this peptide remained on the membrane.[29] To validate that the addition of JB858 will not affect BACE1 activity, a kinetic assay was performed with different BACE1 concentrations (0, 70, 350, and 900 nM) and in the presence of 0 or 4 equiv of JB858, along with the enzyme substrate and blocking peptides (Figure 5). An increase of the ratio QD/Cy3B was observed, which indicates that the probe is being successfully cleaved by the enzyme. Moreover, an enzyme concentration-dependent effect can be observed, though perhaps not unexpectedly the sensor with the JB858 did result in slightly inhibited activity (15−20%, see Figure S5). We assign this lower activity to the steric blocking caused by the comparatively bulky targeting moiety complicating the approach of BACE1 to the QD bound substrate.

Monitoring BACE1 Activity in Living Cells. We explored the suitability of our developed sensor to monitor BACE1 activity in living cells; therefore, we chose the neuroblastoma cell line SH-SY5Y to monitor the proteolytic activity. This cellular line physiologically expresses BACE1 and represents a widely used platform to test several drug candidates in the neurodegeneration field.[40,41] For the microscopy imaging, we began by qualitative confirmation that the membrane-targeted QD (i.e., without BACE1 substrate peptides) was nontoxic to the cells (e.g., cellular morphology and confluence) and that the QD was able to incorporate inside the cells and be detected. We then performed time-lapse experiments comparing untreated cells (background cell autofluorescence) with the sensor and sensor with verubecestat added to the cells in order to confirm not only the activity of the sensor but also its ability to monitor the presence of BACE1 inhibitors. Cells were incubated with the sensors (40 nM QD functionalized with 2 μM JB858 and 160 nM substrate peptide) and the inhibitor (1 nM), and emission luminescence of the QD and Cy3B was acquired at 60, 90, and 120 min. Fluorescence density was acquired from the automatically selected region of interest based on the bright field appearance of the cells, and the data corresponding to the

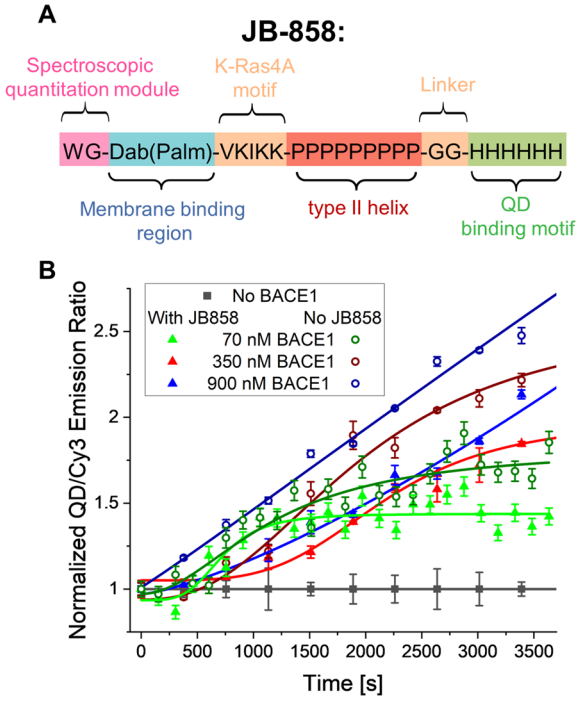

Figure 5. Membrane insertion peptide and BACE1 kinetic assays. (A) Peptide sequence of JB858 peptide with its functional regions differentiated by color. Dab(Palm) is a diaminobutyric acid with an attached palmitoyl group. (B) BACE1 kinetic assay with different BACE1 concentrations in the presence (filled triangles) or absence (empty circles) of four equiv of the membrane anchor peptide JB858 conjugated to the QD surface. The QD/Cy3B ratio was monitored over time and normalized to t_0. Uncertainties arise from triplicate measurements. Data are represented as mean ± SD.

fluorescence emission of the QD and Cy3B was analyzed. Similar to what was observed *in vitro*, the presence of BACE1 expressed by the SH-SY5Y cells resulted in an increased QD emission. When verubecestat was added to the cells, fluorescence values did not increase, suggesting that the QD emission increase was specific and linked to BACE1 activity (Figure 6). Fluorescence variation within each condition was also calculated, only observing an emission increase for the QD sensor without the addition of the BACE1 inhibitor (Figure

https://doi.org/10.1021/acsami.4c12560
ACS Appl. Mater. Interfaces 2024, 16, 63186−63194

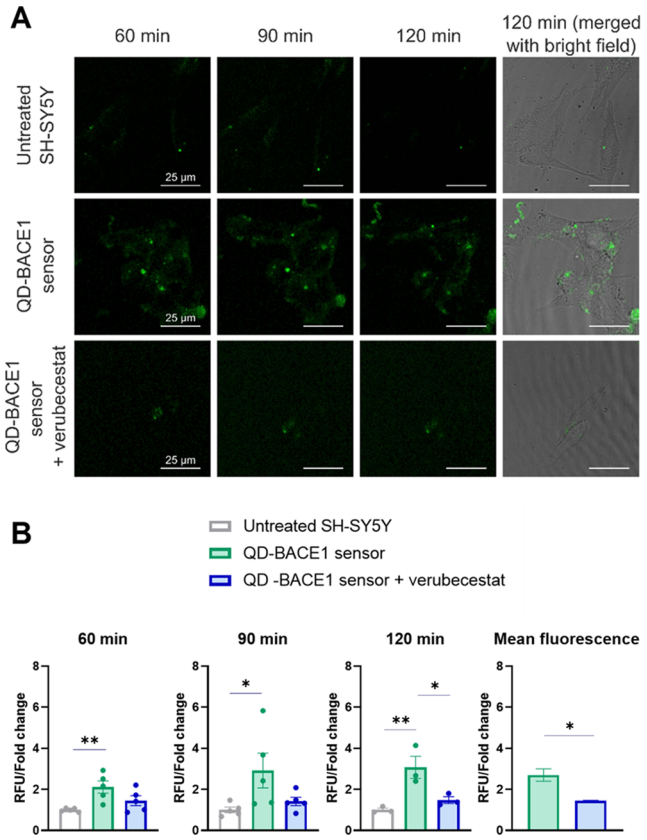

Figure 6. (A) Time-lapse images of SH-SY5Y cells with the QD-BACE1 sensor imaged at 63× magnification. (B) Normalized fluorescence density QD integrated luminescence ($\lambda_{ex/em}$ = 405/496−560 nm) increase is not observed upon the treatment with BACE1 inhibitor verubecestat. At time 60 min untreated n = 5 individual experiments; QD-BACE1 n = 5 individual experiments; QD-BACE1 with 1 nM verubecestat n = 6 individual experiments. At 90 min, untreated n = 5 individual experiments; QD-BACE1 n = 5 individual experiments; QD-BACE1 with 1 nM verubecestat n = 5 individual experiments. At 120 min, untreated n = 3 individual experiments; QD-BACE1 n = 3 individual experiments; QD-BACE1 with 1 nM verubecestat n = 3 individual experiments. Data are represented as mean ± SEM. Significance levels of comparison between groups were calculated using Ordinary One-way ANOVA with Dunnett's multiple comparison test, and stated as follows: *p < 0.05; **p < 0.01. In the cases in which no mark is set, it denotes nonsignificance.

S6). These experiments clearly distinguish the cellular response with or without the inhibitor added, confirming the functionality of the sensor as an *in cellulo* BACE1 inhibitor assay.

CONCLUSIONS

Accurately sensing key molecular processes both *in vitro* and inside cells provides illuminating knowledge of cellular processes at the molecular level. Specifically, protease sensing has benefited from QD-based sensors, helping understand protease's roles in physiology along with their role in several pathological conditions. We have demonstrated the utilization of QD-based FRET sensors as a probe for the critical BACE1 enzyme. BACE1 is a key target in Alzheimer's research, yet remains little understood, in part due to the lack of optimal probes that can both assay enzyme modifiers in a high-throughput manner as well as characterize the *in cellulo* and *in vivo* effects of treatment on BACE1 activity. This lack of development has been due in part to the complicated nature of the enzyme's activity, requiring both stability at lower pH as well as targeting of the cellular membrane. We exploited QDs as a means of creating a bright sensitive FRET probe capable of working at nanomolar concentrations of the probe and detecting enzyme activity below 10 nM for multiwell plate assays, obtaining similar enzyme kinetic results as those reported in the literature. Similarly, we were able to utilize our QD probe to look at verubecestat, a BACE1 inhibitor, and obtain a K_i value in line with literature values. The key aspect of the probe was that the QD is not only an excellent FRET donor but due to its relatively large surface area can be functionalized with surface-bound moieties to optimize its stability in the acidic conditions required for BACE1 activity as well as those that target to the cellular membrane. We utilized the optimized sensor to validate the sensors' capability in reporting on SH-SY5Y cells' BACE1 activity and the diminished activity upon incubation with a BACE1 inhibitor. These initial proof-of-concept experiments will allow protocol optimization and begin to answer the many questions that remain around BACE1 enzymatic function in neurodegenerative diseases.

MATERIALS AND METHODS

QD and Ligand Synthesis. The CdSe/CdS/ZnS core/shell/shell QDs and CL4 were synthesized as previously reported.[27,34] The SO_3 ligand was synthesized in two steps as follows: thioctic acid (2.00 g, 9.79 mmol), *N*-hydroxysuccinimide (1.45 g, 12.6 mmol), and dicyclohexylcarbodiimide (2.60 g, 12.6 mmol) were placed in a 250 mL round-bottom flask and purged with N_2. Acetonitrile (100 mL) was added to the mixture, and the mixture was stirred overnight at room temperature. The reaction mixture was filtered through Celite and concentrated to dryness under vacuum. The crude product, TA-NHS, was purified by chromatography on silica gel with CH_2Cl_2/MeCN (30:1) as the eluent. Yield = 1.85 g (63%). ^{1}H NMR (400 MHz, $CDCl_3$): δ 3.58 (m, 1H), 3.15 (m, 2H), 2.85 (s, 4H), 2.63 (t, J = 7.4 Hz, 2H), 2.48 (m, 1H), 1.95 (m, 1H), 1.88−1.50 (m, 6H). TA-sulfonate was produced by placing taurine (0.132 g, 1.05 mmol) in a 100 mL round-bottomed flask, followed by THF (3 mL) and NEt_3 (516 μL, 3.70 mmol). The mixture was stirred and slowly dissolved by adding DI water (3 mL). Separately, TA-NHS (0.281 g, 0.926 mmol) was suspended in THF (7 mL) via sonication, slowly added to the reaction mixture, and stirred at room temperature for 3 days under N_2. The solvent was removed under a vacuum, and the crude product was purified by chromatography on silica gel with CH_2Cl_2/MeOH (5:1) with 1% NEt_3. Yield = 0.32 g (83%). ^{1}H NMR (400 MHz, $CDCl_3$): δ 6.98 (br s, 1H), 3.72 (m, 2H), 3.56 (m, 1H), 3.21−3.07 (m, 2H), 3.14 (q, J = 7.5 Hz, 6H), 2.97 (m, 2H), 2.44 (m, 1H), 2.18 (t, J = 7.6 Hz, 2H), 1.91 (m, 1H), 1.67 (m, 4H), 1.46 (m, 2H), 1.83 (t, J = 7.4 Hz, 9H).

Ligand exchange of QDs with CL4 and SO_3 was performed as described previously.[27,42]

Peptide Synthesis. BACE1 substrate and membrane anchor peptides were automatically chain-assembled by fluorenylmethoxycarbonyl protecting group (Fmoc)-solid phase peptide synthesis (SPSS) with a peptide synthesizer using 0.1 mmol of H-Rink-Amide-ChemMatrix resin with a loading capacity of 0.49 mmol g^{-1} (Biotage). Fmoc-protected amino acids were dissolved in *N*-methylpyrrolidone and a standard coupling was performed with 10 equiv of *N*,*N*-diisopropylethylamine and 7 equiv of *o*-(1-benzotriazol-1-yl)-1,1,3,3-tetramethyluronium hexafluorophosphate for 45 min with 7 equiv of amino acid. After coupling, resin was acetylated and treated with a cleavage cocktail composed of 92.5% trifluoroacetic acid (TFA), 2.5% 1,2-ethanedithiol, 2.5% triisopropylsilane, and 2.5% H_2O for 120 min. Then, resins were filtered, and TFA was evaporated with a gentle N_2 flow. The crude peptides were precipitated with cold

https://doi.org/10.1021/acsami.4c12560
ACS Appl. Mater. Interfaces 2024, 16, 63186−63194

ether and centrifuged at 7,000 rpm for 10 min. Ether was discarded, and the pellet was dissolved in 30% buffer B (0.1% TFA, 90% CH_3CN, 10% H_2O) in buffer A (0.05% TFA in H_2O) and lyophilized. Peptides were characterized by HPLC-MS using a C18 column 3.5 μm (4.6 × 150 mm, Waters) and a gradient of 5% to 95% acetonitrile with 0.1% formic acid in water. Membrane anchor peptide JB858 was synthesized and purified as previously described.[29]

Peptide Labeling with Cy3B. BACE1 substrate peptide was dissolved in 50 mM $NaHCO_3$ at pH 7.0 to reach a final concentration of 1.5 mg mL^{-1}. Then, 1.5 equiv of the Cy3B monoreactive maleimide (Thermo Fisher Scientific) dissolved in DMSO was added and the final pH was adjusted to 7.5. Mixtures were incubated under stirring conditions at room temperature for 3 h or overnight. Purification of Cy3B-labeled peptide was carried out using Ni-NTA affinity columns and then RP18 oligopurification cartridge (Applied Biosystems).[21] Peptides were characterized by UV−vis absorbance spectroscopy, lyophilized, and stored at −20 °C.

Sensor Preparation. CL4-QD or SO_3-QD was incubated at a final concentration of 150 nM with different equivalents, 0−6 of the BACE1 substrate peptide labeled with the Cy3B dye for 30 min at room temperature in different buffers (sodium acetate 50 mM pH 4.5, HEPES 50 mM pH 5.0, MES 50 mM pH 5.2, and PBS pH 6.0). For the blocking peptides, CL4-QDs were first incubated for 30 min with 2 equiv of the Cy3B-labeled BACE1 substrate peptide, followed by 15 min of incubation with 0, 20, 30, or 40 equiv of the blocking peptide in the different buffers assayed. To form the membrane-bound sensor, QDs were simultaneously incubated with 4 equiv of BACE1 substrate peptide Cy3B-labeled and 4 equiv of JB858 for 30 min, followed by 15 min incubation with 20 equiv of the blocking peptide in sodium acetate 50 mM pH 4.5. Fluorescence spectra from 500 to 750 nm were recorded by exciting samples at 405 nm in a microplate reader (TECAN Spark).

BACE1 Kinetic Assay *In Vitro*. Sodium acetate, MES, HEPES, and PBS buffers were tested for quenching efficacy and BACE1 digestion, and sodium acetate buffer was selected for further studies. In the same way, CL4-QDs were found to be the preferred choice. CL4-QDs were mixed with 4 equiv of BACE1 Cy3B-labeled substrate peptide for 30 min and with 20 equiv of the blocking peptide for 15 min in 50 mM sodium acetate buffer pH 4.5 at a final concentration of 15 nM. In the case of the membrane-bound sensor, QDs were additionally incubated with 4 equiv of the membrane targeting peptide JB858. After incubation, the Cy3B-peptide-QD conjugates were incubated with increasing concentrations of BACE1 (0, 10, 25, 50, 150, 300 nM) at 37 °C and the fluorescence emission at 545 and 580 nm was collected after excitation at 405 nm in a microplate reader (TECAN Spark). Photoluminescence measurements were collected at 30 s intervals and finished at 3600 s (60 min). All experiments were performed in triplicate.

For the inhibition with verubecestat (Sigma-Aldrich), increasing concentrations of the drug (0, 0.01, 0.1, 0.25, 0.5, 1, 2.5, 5, 7.5, 10, 50, and 100 nM) were previously incubated with BACE1 (150 nM) at 37 °C for 30 min. The k_{cat}/K_M value was calculated using Originlab software based on the assumption that the system could be properly fit by a Michaelis−Menten equation.[22] The verubecestat K_i value was calculated using OriginLab software from a dose-dependent inhibition curve.

BACE1 Kinetic Assay in Living Cells. Human neuroblastoma SH-SY5Y cells (obtained from the European Collection of Authenticated Cell Cultures, ECACC, Health Protection Agency) were cultured in Dulbecco's Modified Eagle Medium (DMEM, Gibco) supplemented with 10% fetal bovine serum (FBS, Gibco) and 1% penicillin/streptomycin (Gibco) in a humidified 5% CO_2 incubator at 37 °C.

For the BACE1 assay, 10^5 cells were seeded per well in a μ-slide 8-well plate. At 24 h, cells were pretreated with 1 nM verubecestat or the corresponding volume of DMSO for 1 h. During the pretreatment, the QD was incubated with the membrane peptide and the substrate peptide in PBS to achieve a final concentration of 40 nM QD, 2 μM membrane peptide and 160 nM substrate peptide after the dilution in DMEM without phenol red supplemented with 10% FBS and 1% penicillin/streptomycin. Subsequent to the pretreatment, the cells were incubated with the sensor for 1 h, washed 3 times in PBS, and left in culture media for the imaging.

Confocal Laser Scanning Microscopy. Confocal microscopy experiments were performed using a Confocal Stellaris 8 instrument with a Leica HC PL APO CS2 63×/1.20 (water) objective. For each well, at least 3 different fields of view were selected with a 184.70 μm width, 184.70 μm height, and 5 μm depth over 10 stacks. The samples were excited with a 405 nm wavelength laser. The emission was collected at 496−560 nm for the QD and at 580−657 nm for the Cy3B.

Quantitative Analysis of *In Cellulo* Sensor Activity. Quantitative analysis of the images was performed by integrating the fluorescence density corresponding to the QD and plotting the images as a function of time. Each image was acquired at 63× magnification and represents a size of 184.70 × 184.70 μm in a resolution of 5.5440 pixels per μm (1024 × 1024). For each field of view, 10 stacks were recorded. Images were obtained from a total of five independent experiments for the 60 and 90 min time points and from three independent experiments for the 120 min time points. To process the image, the region of interest was automatically selected based on the bright field appearance of the cells. The minimum and maximum pixel values were set to 250 and 1750, respectively, for a better visualization of the image. Then the pixel value was measured for each channel, and the integrated density was used to analyze the data. Individual experiment counts are provided in the Figure 6 caption. Each individual experiment contains an average data set of 23 measurements per condition and time point represented in the graph. Each measurement corresponds to an individual cell or small group of contiguous cells from 3/4 different fields of view. The ROUT method (Q = 10%) was used to identify the technical outliers of the data of all experiments for the same time point. For each experiment, after the outliers were removed, the mean was normalized by the mean of untreated cells and represented as a data point. The mean of each time point (60, 90, and 120 min) was also represented as the mean fluorescence to compare the conditions of QD-BACE1 sensor with and without verubecestat.

■ ASSOCIATED CONTENT

Supporting Information

The Supporting Information is available free of charge at https://pubs.acs.org/doi/10.1021/acsami.4c12560.

Fluorescence spectra showing QD-Cy3B FRET in varying buffers and with varying QD ligands, increased sensor stability through the use of blocking peptide ligands, representative data of enzyme kinetics, steric inhibition of JB858 on BACE1 activity, additional cell images analysis, assay conditions optimization table (PDF)

■ AUTHOR INFORMATION

Corresponding Authors

Sebastián A. Díaz − *Center for Bio/Molecular Science and Engineering, Code 6900, U.S. Naval Research Laboratory, Washington, DC 20375, United States;* orcid.org/0000-0002-5568-0512; Email: sebastian.diaz@nrl.navy.mil

Valle Palomo − *Instituto Madrileño de Estudios Avanzados en Nanociencia (IMDEA Nanociencia), 28049 Madrid, Spain; Centro de Investigación Biomédica en Red en Enfermedades Neurodegenerativas, (CIBERNED), Instituto de Salud Carlos III, 28029 Madrid, Spain; Unidad Asociada al Centro Nacional de Biotecnología (CSIC), 28049 Madrid, Spain;* orcid.org/0000-0002-1473-4086; Email: valle.palomo@imdea.org

https://doi.org/10.1021/acsami.4c12560
ACS Appl. Mater. Interfaces 2024, 16, 63186−63194

Authors

Carlota Tosat-Bitrián − *Centro de Investigaciones Biológicas "Margarita Salas"-CSIC, 28040 Madrid, Spain; Centro de Investigación Biomédica en Red en Enfermedades Neurodegenerativas, (CIBERNED), Instituto de Salud Carlos III, 28029 Madrid, Spain*

Jesús Alejandro Bueso de Barrio − *Instituto Madrileño de Estudios Avanzados en Nanociencia (IMDEA Nanociencia), 28049 Madrid, Spain;* orcid.org/0009-0005-4956-5453

Michael H. Stewart − *Optical Sciences Division, Code 5600, U.S. Naval Research Laboratory, Washington, DC 20375, United States*

Kimihiro Susumu − *Optical Sciences Division, Code 5600, U.S. Naval Research Laboratory, Washington, DC 20375, United States*

Igor L. Medintz − *Center for Bio/Molecular Science and Engineering, Code 6900, U.S. Naval Research Laboratory, Washington, DC 20375, United States;* orcid.org/0000-0002-8902-4687

Complete contact information is available at: https://pubs.acs.org/10.1021/acsami.4c12560

Author Contributions

The manuscript was written through contributions of all authors. All authors have given approval to the final version of the manuscript.

Funding

This work was partially funded by grant RYC2019-027489-I, funded by MCIN/AEI/10.13039/501100011033 and by FSE "invierte en tu futuro". CTB thanks Ministerio de Educación (FPU18/06310) for the predoctoral fellowship and the Office of Naval Research Global for a Visiting Scientist Program fellowship. JAB thanks MCIN/AEI/10.13039/501100011033 and FSE "invierte en tu futuro" for his predoctoral funding (PRE2022-102052) within the project CEX2020-001039-S-20-5. MHS, KS, ILM, and SAD acknowledge support from the Office of Naval Research, programmatic funding from the US Naval Research Laboratory (NRL), and the NRL Nanosciences Institute.

Notes

The authors declare no competing financial interest.

■ ACKNOWLEDGMENTS

The authors acknowledge the technical assistance and advice of Ana Oña Blanco, Gianluca D'Agostino and Jaime Fernández de Córdoba, Advanced Optical Microscopy Facility (CNB-CSIC).

■ REFERENCES

(1) Cole, S. L.; Vassar, R. The Role of Amyloid Precursor Protein Processing by BACE1, the β-Secretase, in Alzheimer Disease Pathophysiology. *J. Biol. Chem.* **2008**, *283* (44), 29621−29625.

(2) Willem, M.; Garratt, A. N.; Novak, B.; Citron, M.; Kaufmann, S.; Rittger, A.; DeStrooper, B.; Saftig, P.; Birchmeier, C.; Haass, C. Control of Peripheral Nerve Myelination by the ß-Secretase BACE1. *Science* **2006**, *314* (5799), 664−666.

(3) He, W.; Hu, J.; Xia, Y.; Yan, R. β-Site Amyloid Precursor Protein Cleaving Enzyme 1(BACE1) Regulates Notch Signaling by Controlling the Cleavage of Jagged 1 (Jag1) and Jagged 2 (Jag2) Proteins. *J. Biol. Chem.* **2014**, *289* (30), 20630−20637.

(4) Das, B.; Yan, R. Role of BACE1 in Alzheimer's synaptic function. *Transl. Neurodegener.* **2017**, *6* (1), 23.

(5) Meakin, P. J.; Mezzapesa, A.; Benabou, E.; Haas, M. E.; Bonardo, B.; Grino, M.; Brunel, J.-M.; Desbois-Mouthon, C.; Biddinger, S. B.; Govers, R.; et al. The beta secretase BACE1 regulates the expression of insulin receptor in the liver. *Nat. Commun.* **2018**, *9* (1), 1306.

(6) Lange, J.; Lunde, K. A.; Sletten, C.; Møller, S. G.; Tysnes, O.-B.; Alves, G.; Larsen, J. P.; Maple-Grødem, J. Association of a *BACE1* Gene Polymorphism with Parkinson's Disease in a Norwegian Population. *Parkinson's Dis.* **2015**, *2015*, No. 973298.

(7) Koistinen, H.; Prinjha, R.; Soden, P.; Harper, A.; Banner, S. J.; Pradat, P.-F.; Loeffler, J.-P.; Dingwall, C. Elevated levels of amyloid precursor protein in muscle of patients with amyotrophic lateral sclerosis and a mouse model of the disease. *Muscle Nerve* **2006**, *34* (4), 444−450.

(8) Nozal, V.; García-Rubia, A.; Cuevas, E. P.; Pérez, C.; Tosat-Bitrián, C.; Bartolomé, F.; Carro, E.; Ramírez, D.; Palomo, V.; Martínez, A. From Kinase Inhibitors to Multitarget Ligands as Powerful Drug Leads for Alzheimer's Disease using Protein-Templated Synthesis. *Angew. Chem., Int. Ed.* **2021**, *60* (35), 19344−19354.

(9) Nishitomi, K.; Sakaguchi, G.; Horikoshi, Y.; Gray, A. J.; Maeda, M.; Hirata-Fukae, C.; Becker, A. G.; Hosono, M.; Sakaguchi, I.; Minami, S. S.; et al. BACE1 inhibition reduces endogenous Abeta and alters APP processing in wild-type mice2. *J. Neurochem.* **2006**, *99* (6), 1555−1563.

(10) Mullard, A. BACE failures lower AD expectations, again. *Nat. Rev. Drug Discovery* **2018**, *17* (6), 385−385.

(11) Taylor, H. A.; Przemylska, L.; Clavane, E. M.; Meakin, P. J. BACE1: More than just a β-secretase. *Obes. Rev.* **2022**, *23* (7), No. e13430.

(12) Chang, Z.; Zhu, B.; Liu, J.; Dong, H.; Hao, Y.; Zhou, Y.; Travas-Sejdic, J.; Xu, M. "Signal-on" electrochemical detection of BACE1 for early detection of Alzheimer's disease. *Cell Rep. Phys. Sci.* **2024**, *5*, 101632.

(13) Lu, J.; Zhang, Z.; Yang, J.; Chu, J.; Li, P.; Zeng, S.; Luo, Q. Visualization of β-secretase cleavage in living cells using a genetically encoded surface-displayed FRET probe. *Biochem. Biophys. Res. Commun.* **2007**, *362* (1), 25−30.

(14) Folk, D. S.; Torosian, J. C.; Hwang, S.; McCafferty, D. G.; Franz, K. J. Monitoring β-Secretase Activity in Living Cells with a Membrane-Anchored FRET Probe. *Angew. Chem., Int. Ed.* **2012**, *51* (43), 10795−10799.

(15) Zhao, L.; Zhao, Y.; Tang, F.-L.; Xiong, L.; Su, C.; Mei, L.; Zhu, X.-J.; Xiong, W.-C. pHluorin-BACE1-mCherry Acts as a Reporter for the Intracellular Distribution of Active BACE1 *In Vitro* and *In Vivo*. *Cells* **2019**, *8* (5), 474.

(16) Ma, F.; Wang, Q.; Xu, Q.; Zhang, C. Y. Self-Assembly of Superquenched Gold Nanoparticle Nanosensors for Lighting up BACE-1 in Live Cells. *Anal. Chem.* **2021**, *93* (45), 15124−15132.

(17) Wegner, K. D.; Hildebrandt, N. Quantum dots: bright and versatile in vitro and in vivo fluorescence imaging biosensors. *Chem. Soc. Rev.* **2015**, *44* (14), 4792−4834.

(18) Hildebrandt, N.; Spillmann, C. M.; Algar, W. R.; Pons, T.; Stewart, M. H.; Oh, E.; Susumu, K.; Díaz, S. A.; Delehanty, J. B.; Medintz, I. L. Energy Transfer with Semiconductor Quantum Dot Bioconjugates: A Versatile Platform for Biosensing, Energy Harvesting, and Other Developing Applications. *Chem. Rev.* **2017**, *117* (2), 536−711.

(19) Zhang, Q.; Gao, X.; Ho, Y. P.; Liu, M.; Han, Y.; Li, D. L.; Yuan, H. M.; Zhang, C. Y. Controllable Assembly of a Quantum Dot-Based Aptasensor Guided by CRISPR/Cas12a for Direct Measurement of Circulating Tumor Cells in Human Blood. *Nano Lett.* **2024**, *24* (7), 2360−2368.

(20) Zhang, Q.; Liu, H.; Xu, Q.; Liu, H.; Han, Y.; Li, D.-L.; Ma, F.; Zhang, C.-Y. Construction of a 3D Quantum Dot Nanoassembly with Two-Step FRET for One-Step Sensing of Human Telomerase RNA in Breast Cancer Cells and Tissues. *Anal. Chem.* **2024**, *96* (19), 7738−7746.

(21) Díaz, S. A.; Breger, J. C.; Medintz, I. L. Monitoring Enzymatic Proteolysis Using Either Enzyme- or Substrate-Bioconjugated

Quantum Dots. In *Methods in Enzymology*; Kumar, C. V., Ed.; Academic Press, 2016; Vol. *571*, pp 19−54.
(22) Díaz, S. A.; Malonoski, A. P.; Susumu, K.; Hofele, R. V.; Oh, E.; Medintz, I. L. Probing the kinetics of quantum dot-based proteolytic sensors. *Anal. Bioanal. Chem.* **2015**, *407* (24), 7307−7318.
(23) Palomo, V.; Díaz, S. A.; Stewart, M. H.; Susumu, K.; Medintz, I. L.; Dawson, P. E. 3,4-Dihydroxyphenylalanine Peptides as Non-perturbative Quantum Dot Sensors of Aminopeptidase. *ACS Nano* **2016**, *10* (6), 6090−6099.
(24) Breger, J. C.; Susumu, K.; Lasarte-Aragonés, G.; Díaz, S. A.; Brask, J.; Medintz, I. L. Quantum Dot Lipase Biosensor Utilizing a Custom-Synthesized Peptidyl-Ester Substrate. *ACS Sens.* **2020**, *5* (5), 1295−1304.
(25) Green, C. M.; Spangler, J.; Susumu, K.; Stenger, D. A.; Medintz, I. L.; Díaz, S. A. Quantum Dot-Based Molecular Beacons for Quantitative Detection of Nucleic Acids with CRISPR/Cas(N) Nucleases. *ACS Nano* **2022**, *16* (12), 20693−20704.
(26) Green, C. M.; Mathur, D.; Susumu, K.; Oh, E.; Medintz, I. L.; Díaz, S. A. Polyhistidine-Tag-Enabled Conjugation of Quantum Dots and Enzymes to DNA Nanostructures. In *Bioluminescence: Methods and Protocols*; Kim, S.-B., Ed.; Springer: US, 2022; Vol. *2*, pp 61−91.
(27) Susumu, K.; Oh, E.; Delehanty, J. B.; Blanco-Canosa, J. B.; Johnson, B. J.; Jain, V.; Hervey, W. J. I. V.; Algar, W. R.; Boeneman, K.; Dawson, P. E.; et al. Multifunctional Compact Zwitterionic Ligands for Preparing Robust Biocompatible Semiconductor Quantum Dots and Gold Nanoparticles. *J. Am. Chem. Soc.* **2011**, *133* (24), 9480−9496.
(28) Choi, Y.; Cho, Y.; Kim, M.; Grailhe, R.; Song, R. Fluorogenic Quantum Dot-Gold Nanoparticle Assembly for Beta Secretase Inhibitor Screening in Live Cell. *Anal. Chem.* **2012**, *84* (20), 8595−8601.
(29) Boeneman, K.; Delehanty, J. B.; Blanco-Canosa, J. B.; Susumu, K.; Stewart, M. H.; Oh, E.; Huston, A. L.; Dawson, G.; Ingale, S.; Walters, R.; et al. Selecting Improved Peptidyl Motifs for Cytosolic Delivery of Disparate Protein and Nanoparticle Materials. *ACS Nano* **2013**, *7* (5), 3778−3796.
(30) Tomasselli, A. G.; Qahwash, I.; Emmons, T. L.; Lu, Y.; Leone, J. W.; Lull, J. M.; Fok, K. F.; Bannow, C. A.; Smith, C. W.; Bienkowski, M. J.; et al. Employing a superior BACE1 cleavage sequence to probe cellular APP processing. *J. Neurochem.* **2003**, *84* (5), 1006−1017.
(31) Folk, D. S.; Franz, K. J. A Prochelator Activated by β-Secretase Inhibits Aβ Aggregation and Suppresses Copper-Induced Reactive Oxygen Species Formation. *J. Am. Chem. Soc.* **2010**, *132* (14), 4994−4995.
(32) Cooper, M.; Ebner, A.; Briggs, M.; Burrows, M.; Gardner, N.; Richardson, R.; West, R. Cy3B: Improving the Performance of Cyanine Dyes. *J. Fluoresc.* **2004**, *14* (2), 145−150.
(33) Green, C. M.; Hastman, D. A.; Mathur, D.; Susumu, K.; Oh, E.; Medintz, I. L.; Díaz, S. A. Direct and Efficient Conjugation of Quantum Dots to DNA Nanostructures with Peptide-PNA. *ACS Nano* **2021**, *15* (5), 9101−9110.
(34) Rogers, K. E.; Nag, O. K.; Stewart, M. H.; Susumu, K.; Oh, E.; Delehanty, J. B. Multivalent Display of Erythropoietin on Quantum Dots Enhances Aquaporin-4 Expression and Water Transport in Human Astrocytes In Vitro. *Bioconjugate Chem.* **2023**, *34* (12), 2205−2214.
(35) Díaz, S. A.; Sen, S.; Boeneman Gemmill, K.; Brown, C. W., III; Oh, E.; Susumu, K.; Stewart, M. H.; Breger, J. C.; Lasarte Aragonés, G.; Field, L. D.; et al. Elucidating Surface Ligand-Dependent Kinetic Enhancement of Proteolytic Activity at Surface-Modified Quantum Dots. *ACS Nano* **2017**, *11* (6), 5884−5896.
(36) Gemmill, K. B.; Díaz, S. A.; Blanco-Canosa, J. B.; Deschamps, J. R.; Pons, T.; Liu, H.-W.; Deniz, A.; Melinger, J.; Oh, E.; Susumu, K.; et al. Examining the Polyproline Nanoscopic Ruler in the Context of Quantum Dots. *Chem. Mater.* **2015**, *27* (18), 6222−6237.
(37) Green, C. M.; Hastman, D. A.; Susumu, K.; Spangler, J.; Stenger, D. A.; Medintz, I. L.; Díaz, S. A. Passivating quantum dots against histag-displaying enzymes using blocking peptides: salient considerations for self-assembling quantum dot biosensors. *Sens. Diagn.* **2023**, *2* (6), 1521−1530.
(38) Kennedy, M. E.; Stamford, A. W.; Chen, X.; Cox, K.; Cumming, J. N.; Dockendorf, M. F.; Egan, M.; Ereshefsky, L.; Hodgson, R. A.; Hyde, L. A.; et al. The BACE1 inhibitor verubecestat (MK-8931) reduces CNS β-amyloid in animal models and in Alzheimer's disease patients. *Sci. Transl. Med.* **2016**, *8* (363), 363ra150−363ra150.
(39) Kandalepas, C. P.; Vassar, R. The Normal and Pathologic Roles of the Alzheimer's β-secretase, BACE1. *Curr. Alzheimer Res.* **2014**, *11* (5), 441−449.
(40) Huang, P.; Zheng, N.; Zhou, H.-b.; Huang, J. Curcumin inhibits BACE1 expression through the interaction between ERβ and NFκB signaling pathway in SH-SY5Y cells. *Mol. Cell. Biochem.* **2020**, *463* (1), 161−173.
(41) Nopparat, C.; Chaopae, W.; Boontem, P.; Sopha, P.; Wongchitrat, P.; Govitrapong, P. Melatonin Attenuates High Glucose-Induced Changes in Beta Amyloid Precursor Protein Processing in Human Neuroblastoma Cells. *Neurochem. Res.* **2022**, *47* (9), 2568−2579.
(42) Jin, H.; Nam, J.; Park, J.; Jung, S.; Im, K.; Hur, J.; Park, J.-J.; Kim, J.-M.; Kim, S. Strong polyelectrolyte quantum dot surface for stable bioconjugation and layer-by-layer assembly applications. *Chem. Commun.* **2011**, *47* (6), 1758−1760.

https://doi.org/10.1021/acsami.4c12560
ACS Appl. Mater. Interfaces 2024, 16, 63186−63194